

A model for the dynamics and internal structure of planar doping fronts in organic semiconductors

M. Modestov, V. Bychkov, D. Valiev, and M. Marklund*
Department of Physics, Umeå University, SE-901 87 Umeå, Sweden

The dynamics and internal structure of doping fronts in organic semiconductors are investigated theoretically using an extended drift-diffusion model for ions, electrons and holes. The model also involves the injection barriers for electrons and holes in the partially doped regions in the form of the Nernst equation, together with a strong dependence of the electron and hole mobility on concentrations. Closed expressions for the front velocities and the ion concentrations in the doped regions are obtained. The analytical theory is employed to describe the acceleration of the p- and n-fronts towards each other. The analytical results show very good agreement with the experimental data. Furthermore, it is shown that the internal structure of the doping fronts is determined by the diffusion and mobility processes. The asymptotic behavior of the concentrations and the electric field is studied analytically inside the doping fronts. The numerical solution for the front structure confirms the most important predictions of the analytical theory: a sharp head of the front in the undoped region, a smooth relaxation tail in the doped region, and a plateau at the critical point of transition from doped to undoped regions.

I. INTRODUCTION

Organic semiconductors (OSCs) demonstrate a number of interesting properties, which distinguish them from crystalline inorganic semiconductors¹⁻³. Among the most intriguing features is the possibility of electrochemical doping by means of reversible redox reactions, demonstrated in a number of materials^{4,5}. The electrochemical doping transforms the OSCs from essentially insulating state to a metallic-like state with the conductivity increased by many orders of magnitude⁶. This transformation is accompanied by a considerable change of the material properties including color, photoluminescence capability, volume, and surface energy^{2,3,5}. The electrochemical doping can be performed straightforward *in situ*, when an OSC coated on a metal electrode is in contact with an electrolyte and is subjected to an appropriate electric potential. In the transformation process, electronic charges (electrons and holes) from the electrode are injected into the OSC and subsequently electrostatically compensated by an influx of respective ions from the electrolyte (cations and anions)⁷⁻⁹.

The opportunity for tuning the electronic and optical properties of OSCs has triggered a number of studies at the fundamental as well as practical aspects of doping. These works in turn paved the way to numerous applications of this process in novel electronic and photonic devices^{1-5,10-13}. A classical example of the electronic devices utilizing the electrochemical doping is polymer based light-emitting electrochemical cells (LECs)^{8,10,14-16}. A LEC comprises an organic semiconductor in a form of conjugated fluorescent polymer, which is blended with a solid state electrolyte. The blend of the conjugated polymer and the electrolyte forms the active material of the LEC and is sandwiched between two electrodes. When an electric potential applied between the electrodes exceeds the band gap potential of the conjugated polymer, then the doping transforma-

tion starts with injected holes and electrons forming the p- and n-type doped regions close to the respective electrodes¹⁷. The doping process in planar LECs can be visualized under ultra-violet illumination since doped OSCs display very high rate of photoluminescence quenching. The doped material in LEC is observed as dark regions quite distinct from the original undoped substance. By employing the ultra-violet visualization, it was demonstrated experimentally that doping transformation in OSC develops in the form of two localized fronts of p- and n-type doping, which emerge at the electrodes and propagate towards each other¹⁶⁻²¹. When the fronts meet, the two doped regions form a p-n junction, which emits a visible light. The purpose of the present work is to provide a theoretical model for the front propagation in LECs prior to the development of the p-n junction.

A number of interesting theoretical works has been devoted to charge dynamics in LECs and other OSC devices^{20,22-27}. In particular, the authors of Refs. 22 and 23 investigated a stationary light-emitting p-n junction as a final state of the doping process in LECs. At this stage of the process, the whole OSC is already converted to the state with high conductivity. However, the non-steady problem of doping front dynamics and structure prior to the formation of the p-n junction is much more difficult to analyze, since it involves transition of the OSC from the undoped weakly conducting state to the metallic-like doped state within the front. As we show in the present paper, the problem includes not only the electrodynamic issues of the OSC plasma motion, but also some questions of thermodynamics and quantum mechanics, which are still waiting for an answer. The problem of front dynamics was addressed in 20 and 21 from the empirical point of view of total OSC conduction: the purpose was to analyze the experimental data without investigating the complicated internal front properties. At the same time, considerable progress has been achieved in the adjacent problem of front dynamics

in one-electrode OSC devices, such as e.g. electrochemical sensors and actuators^{24,26,27}. For example, the recent work by Wang et al.²⁷ provided discussion of all elements required for front formation in the one-electrode devices. The model proposed in Ref. 27 included the Poisson equation, diffusion and mobility (migration) of holes and ions (cations), taking into account possible nonlinear (non-Fickian) character of the transport coefficients. The Nernst equation for light particles, holes, in the region of high conductivity in that case follows from the diffusion-mobility model under the condition of quasi-equilibrium. In a sense, the process studied in Ref. 27 is just the opposite to the doping fronts propagating in LECs. In the doping process in LECs, holes and electrons are injected into the active material by an externally applied electrical field, which helps them overcoming a certain thermodynamic barrier, and dope the active material. The ions, on the other hand, give way to the light charges, and compensate the excessive charge thus avoiding generation of strong internal electric fields. In the devices presented by Wang et al.²⁷ charge motion goes in the opposite direction: the cations advance together with the front, while holes retreat leaving the material. With some caution, the fronts of electrochemical transformation in LECs and in the one-electrode devices²⁷ may be compared to uphill climb and downhill glide, respectively. Still, the physical understanding of front dynamics in the one-electrode devices as presented in²⁷ may be helpful in constructing models of the doping front propagation in LECs. In particular, recent paper²⁸ demonstrated that the theoretical description of doping fronts in LECs requires not only the common diffusion-mobility set of equations, but also nonlinear concentration-dependent transport coefficients for holes/electrons and the thermodynamic injection barrier for the light charges in the form of the Nernst potential.

The present paper develops the ideas of Refs.^{27,28}. Using the theoretical model proposed in²⁸, we study dynamics and internal structure of the doping fronts in LECs. We derive compact analytical formulas for the front velocities depending on the electric field together with the ion concentrations in the doped regions. On the basis of the analytical theory we describe acceleration of the p- and n-fronts approaching each other. The analytical results show very good agreement with the experimental data. We show that the internal structure of the doping fronts is determined by diffusion and mobility processes. We study analytically the asymptotic behavior of the concentrations and the electrical field inside the doping fronts. We also solve numerically for the front structure, and confirm the most important predictions of the analytical theory: a sharp head of the front in the undoped region, a smooth relaxation tail in the doped region, and a plateau at the critical point of transition from doped to undoped regions.

The paper is organized as follows: In Sec. II we introduce the basic equations of the model. In Sec. III we study properties of the doping fronts considered as surfaces of discontinuity; we find the front velocity and ion

concentrations in the doped regions behind the fronts and then describe front acceleration in LECs. Section IV is devoted to the internal structure of the fronts. We discuss characteristic length scales of the process, the condition of quasi-neutrality, and the necessity of an injection barrier for the system of equations. We investigate asymptotic analytical solutions to the equations in the specific zones of the front and, finally, we numerically solve the whole set of equations. The paper is concluded by a brief summary in Sec. V.

II. THE MOBILITY-DIFFUSION APPROACH

In general, the dynamics of the ions is determined by equations of force balance

$$nm \frac{d\mathbf{v}}{dt} = -qn\nabla\phi - k_B T \nabla n - \frac{1}{\tau} nm\mathbf{v}, \quad (1)$$

where $q = \pm e$ is charge of positive/negative ions, m is ion mass, n is concentration, ϕ is potential of an electric field with $\mathbf{E} = -\nabla\phi$, k_B is the Boltzmann constant and T is the polymer temperature, which may be taken constant and uniform. The last term in Eq. (1) takes the average contribution of collisions into account. In the case of organic polymers, the collisions dominate over the inertia terms, which allows the mobility-diffusion approach, giving the velocity according to

$$\mathbf{v}_{\pm} = \mp\mu_{\pm}\nabla\phi - \frac{D_{\pm}}{n_{\pm}}\nabla n_{\pm}, \quad (2)$$

where the mobility is given by $\mu = e\tau/m$, labels \pm correspond to positive and negative ions, respectively, and the diffusion coefficient D is related to mobility using the Einstein relation $\mu = eD/k_B T$. When substituting velocity from Eq. (2) to the continuity equations

$$\frac{\partial n_{\pm}}{\partial t} + \nabla \cdot (n_{\pm}\mathbf{v}_{\pm}) = 0, \quad (3)$$

we arrive to the mobility-diffusion model for ion motion according to

$$\frac{\partial n_{\pm}}{\partial t} - \nabla \cdot [\pm\mu_{\pm}n_{\pm}\nabla\phi + D_{\pm}\nabla n_{\pm}] = 0. \quad (4)$$

The equations for electrons and holes may be presented in a similar way, though in the case of light charges one has to take into account an injection barrier ϕ_N for the electrons and holes in the transition from the doped regions to the undoped ones

$$\frac{\partial n_h}{\partial t} - \nabla \cdot [\mu_h n_h \nabla(\phi - \phi_N) + D_h \nabla n_h] = 0, \quad (5)$$

$$\frac{\partial n_e}{\partial t} - \nabla \cdot [-\mu_e n_e \nabla(\phi - \phi_N) + D_e \nabla n_e] = 0, \quad (6)$$

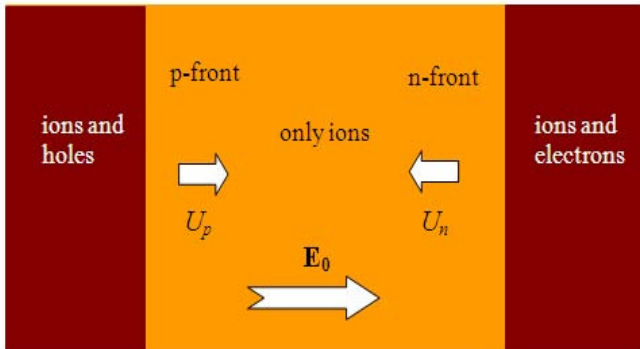


FIG. 1. Schematic of the doping process.

where the labels “h” and “e” stand for holes and electrons, respectively. The barrier originates from quantum and thermodynamic effects, and the interpretation of ϕ_N in terms of an electrostatic force should therefore be done with caution. We discuss the necessity of ϕ_N for self-consistent description of the doping front structure and the particular form of this term in the Section IV. Meanwhile we point out that this term is non-zero only inside the doping fronts, and it should turn to zero in the uniform undoped and doped material ahead of the fronts and behind the fronts, respectively. The electric field obeys the Poisson equation

$$\nabla^2 \phi = (n_- + n_e - n_+ - n_h)e/\epsilon_0. \quad (7)$$

Still, in Section IV we demonstrate that the condition of quasi-neutrality

$$n_- + n_e - n_+ - n_h = 0 \quad (8)$$

holds with a very good accuracy in LECs. We stress that condition (8) *does not* mean constant electric field everywhere. Instead, it implies that even tiny local deviations from zero net charge lead to extremely large electric fields.

III. PROPERTIES OF DISCONTINUOUS DOPING FRONTS

It was demonstrated experimentally^{16,20,21} that the doping process in OSCs happens in a form of two fronts propagating towards each other as shown schematically in Fig. 1. A p-doping front populates the semiconductor with holes, while the n-front makes the semiconductor rich with electrons. Both fronts propagate due to external electric field created by the potential difference between the ends of the semiconductor film. In the present section we consider planar p- and n-fronts as propagating discontinuity surfaces, which transform the original undoped semiconductor to a doped conducting material. To be particular, we start our analysis with a stationary

p-doping front propagating with velocity U_p along the x-axis in a static and uniform electric $E_0 = const$, created in the undoped region by external sources. Looking for the p-front solution in the form $\Psi = \Psi(x - Ut)$ we reduce Eqs. (4), (5), (7) to

$$\frac{d}{dx} \left[-n_h U_p + n_h \mu_h (E - E_N) - D_h \frac{dn_h}{dx} \right] = 0, \quad (9)$$

$$\frac{d}{dx} \left(-n_- U_p - n_- \mu_- E - D_- \frac{dn_-}{dx} \right) = 0, \quad (10)$$

$$\frac{d}{dx} \left(-n_+ U_p + n_+ \mu_+ E - D_+ \frac{dn_+}{dx} \right) = 0, \quad (11)$$

$$\frac{dE}{dx} = e(n_+ - n_- + n_h)/\epsilon_0, \quad (12)$$

where $\mathbf{E}_N \equiv -\nabla \phi_N$ is the effective electric field related to the quantum-thermodynamic injection barrier. Still, in the limit of discontinuous doping fronts considered in the present section, the barrier term does not play any role, since it is zero in the uniform regions both ahead of the front and behind it. Equations (9) – (12) may be integrated analytically across the front. We designate values ahead of the front by the label “0” and values behind the front by “1”. We also take into account that the hole concentration is zero ahead of the front and it reaches some known finite value n_{1h} behind the front. The initial concentrations of positive and negative ions are equal and known, $n_{0-} = n_{0+} = n_0$. Then the parameters in the doped and undoped regions are related by the integrals of Eqs. (9)-(11) according to

$$-U_p + \mu_{h1} E_1 = 0, \quad (13)$$

$$-n_{1+} U_p - n_{1+} \mu_+ E_1 = -n_0 U_p - n_0 \mu_+ E_0, \quad (14)$$

$$-n_{1-} U_p + n_{1-} \mu_- E_1 = -n_0 U_p + n_0 \mu_- E_0, \quad (15)$$

Equation (13) specifies the electric field in the doped region as $E_1 = U_p/\mu_{h1}$, which may be neglected taking into account high mobility of the holes in comparison to the ions in the doped material: $E_1 = U_p/\mu_{h1} \propto (\mu_{\pm}/\mu_{h1})E_0 \ll E_0$. Equation (12) in the uniform doped region determines zero net charge as $n_{1-} - n_{1+} = n_{1h}$. Then equations (14), (15) specify the front velocity and ion concentration in the doped region as

$$U_p = \frac{n_0}{n_{1h}} (\mu_+ + \mu_-) E_0, \quad (16)$$

$$n_{1-} = n_0 + n_{1h} \frac{\mu_-}{\mu_+ + \mu_-}, \quad (17)$$

$$n_{1+} = n_0 - n_{1h} \frac{\mu_+}{\mu_+ + \mu_-}. \quad (18)$$

Similar formulas may be obtained for the n-doping front, i.e.

$$U_n = \frac{n_0}{n_{2e}}(\mu_+ + \mu_-)E_0, \quad (19)$$

$$n_{2+} = n_0 + n_{2e} \frac{\mu_+}{\mu_+ + \mu_-}, \quad (20)$$

$$n_{2-} = n_0 - n_{2e} \frac{\mu_-}{\mu_+ + \mu_-}, \quad (21)$$

where the label “2” designates the conducting substance behind the n-doping front. We note that the p- and n-type doping fronts propagate with different velocities related by

$$U_n = \frac{n_{1h}}{n_{1e}}U_p = \beta U_p. \quad (22)$$

Taking data for electron and hole concentration $n_{1h} = 8.6 \cdot 10^{25} m^{-3}$, $n_{1e} = 1.3 \cdot 10^{26} m^{-3}$ obtained in the experiments^{16,21,28} we find the velocity of the n-front to be less than that of the p-front with $\beta = 0.661$.

Next we consider a semiconductor of finite size with a voltage ϕ_0 applied to the end electrodes and two planar doping fronts moving towards each other. The initial distance between the fronts is L_0 . Since the distance between the fronts $L(t)$ decreases in time and the potential difference is fixed, then electric field $E_0(t)$ in the gap between the fronts grows in time and the fronts accelerate according to Eqs. (16), (19). We designate positions of the fronts by $X_p(t)$, $X_n(t)$. In experiments^{16,21,28}, the n-front (electron doping) starts later, after a time delay t_e ; we thus have two time intervals in the solution: $t < t_e$ and $t > t_e$. We start with the first interval, $t < t_e$, when only the p-front propagates. In that case Eq. (16) for the p-front velocity is reduced to

$$\frac{dX_p}{dt} = \frac{n_0}{n_{1h}}(\mu_+ + \mu_-)\frac{\phi_0}{L} = \frac{U_{p0}}{1 - X_p/L_0} \quad (23)$$

where U_{p0} is the initial velocity of the doping front. Integrating (23) we find

$$\frac{X_p}{L_0} = 1 - \sqrt{1 - 2U_{p0}t/L_0}. \quad (24)$$

At the moment t_e , when the n-front starts, the p-front is already at the position $X_p(t_e)/L_0 = 1 - \sqrt{1 - 2U_{p0}t_e/L_0}$, and we have the reduced distance between the fronts $L_e = L(t_e) = L_0 - X_p(t_e)$. Next, we consider the interval $t > t_e$, when both fronts propagate. In that case the distance between the fronts varies as $L = X_n - X_p$ with

$$\frac{dX_p}{dt} = \frac{U_{p0}}{L/L_0}, \quad \frac{dX_n}{dt} = -\frac{\beta U_{p0}}{L/L_0}, \quad (25)$$

so that

$$\frac{dL}{dt} = -(1 + \beta)\frac{U_{p0}}{L/L_0}. \quad (26)$$

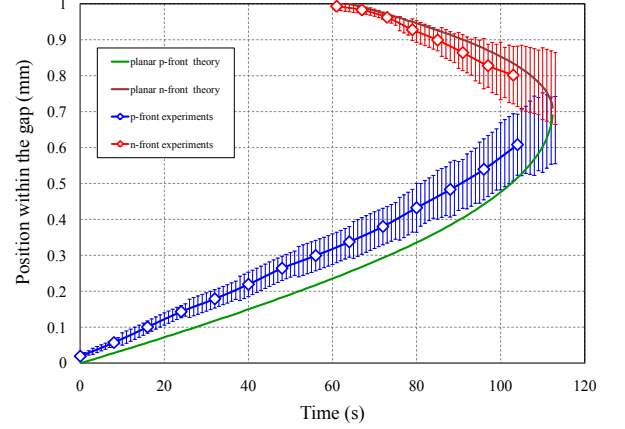


FIG. 2. Positions of the doping fronts versus time as predicted by the analytical theory (solid lines) and obtained experimentally (markers). The uncertainty bars indicate the difference between the fastest and the slowest parts in the multidimensional front structure.

Then, for $t > t_e$, we obtain the solution

$$L(t) = \sqrt{L_e^2 - 2(1 + \beta)U_{p0}L_0(t - t_e)}, \quad (27)$$

$$X_p = X_p(t_e) + \frac{1}{1 + \beta}[L_e - L(t)], \quad (28)$$

$$X_n = L_0 - \frac{\beta}{1 + \beta}[L_e - L(t)]. \quad (29)$$

Figure 2 shows a comparison of the positions of the planar p- and n-fronts, as found analytically through Eqs. (28), (29), to the experimental data. The markers show the average position of the fronts; the error bars indicate the difference between the fastest and the slowest parts of the two-dimensional (2D) front structure (width of the 2D front brush). Such 2D structures develop due to front instabilities, which are beyond the scope of the present paper and which will be presented elsewhere²⁹. Figure 2 indicates that the analytical 1D solution describes the dynamics of the backside of the front structure quite well (within the 10% accuracy of the experimental data). At the same time, the leading parts of the front move noticeably faster than the 1D theory predicts. The last fact demonstrates an important role of the 2D instabilities in the doping front dynamics, which is the subject for the future work.

IV. INTERNAL STRUCTURE OF A DOPING FRONT

A. Basic equations

In the present section we investigate the internal structure of a stationary doping front driven by a constant uniform external electric field E_0 . We start by studying the p-front, since analysis of the n-front is similar. The internal structure of the doping front is controlled by diffusion in Eqs. (9)-(11) integrated within the front

$$-n_h U_p + n_h \mu_h (E - E_N) = D_h \frac{dn_h}{dx}, \quad (30)$$

$$(n_0 - n_-) U_p - \mu_- (n_- E - n_0 E_0) = D_- \frac{dn_-}{dx}, \quad (31)$$

$$(n_0 - n_+) U_p + \mu_+ (n_+ E - n_0 E_0) = D_+ \frac{dn_+}{dx}. \quad (32)$$

A characteristic length scale L_p involved in the problem is determined by the slow diffusion of ions, thus we may choose, e.g., D_- to define

$$L_p \equiv \frac{D_-}{U_p} = \frac{D_- n_{1h}}{(\mu_+ + \mu_-) n_0 E_0}. \quad (33)$$

As an example, taking the experimental data of Refs.^{16,21,28} for $n_{1h} = 8.2 \cdot 10^{25} \text{m}^{-3}$, $n_0 = 3.1 \cdot 10^{26} \text{m}^{-3}$, $\mu_+ = 1.0 \cdot 10^{-10} \text{m}^2/\text{Vs}$, $\mu_- = 2.2 \cdot 10^{-10} \text{m}^2/\text{Vs}$, $T = 360\text{K}$, $E_0 = 3 \cdot 10^3 \text{V/m}$, we can evaluate the characteristic initial p-front velocity as $U_{p0} \approx 3.6 \cdot 10^{-6} \text{m/s}$ and the initial length scale as $L_{p0} \approx 1.8 \cdot 10^{-6} \text{m}$. Still, one has to remember that L_p does not portray the full structure of the doping front. We show below that there are several different characteristic length scales within the front from the undoped to the doped region.

We may also estimate the typical deviations from quasi-neutrality within the front through

$$\frac{n_+ - n_- + n_h}{n_0} \propto \frac{\varepsilon_0}{en_0} \frac{dE}{dx} \propto \frac{\varepsilon_0 E_0}{e L_{p0} n_0} \approx 2.9 \cdot 10^{-10} \ll 1, \quad (34)$$

which allows replacing the Poisson equation Eq. (12) by the condition of quasi-neutrality

$$n_- - n_+ = n_h \quad (35)$$

everywhere within the front with very good accuracy. As a comparison, the electrochemical fronts in the ambipolar devices involve noticeable deviations from quasi-neutrality as shown in Ref.²⁷.

The next important question concerns the terms specifying the injection barrier, ϕ_N , E_N , in Eqs. (5) and (30). Below, we demonstrate that it is indeed impossible to describe the doping front structure without such a barrier term. Let us consider the doped region at the back side

of the front with $\mu_h \gg \mu_{\pm}$. Without the barrier term, one has the force-balance equation

$$n_h m \frac{d\mathbf{v}}{dt} = -en_h \nabla \phi - k_B T \nabla n_h - \frac{n_h m}{\tau} \mathbf{v}. \quad (36)$$

for holes similar to Eq. (1). Within the drift-diffusion approximation, the inertial term $n_h m d\mathbf{v}/dt$ in Eq. (36) is negligible. The characteristic velocities of the doping process are controlled by relatively low ion mobility, Eq. (16). Therefore, by order-of-magnitude the collision term in Eq. (36) is also negligible in comparison with the electric term in the doped region

$$\begin{aligned} \frac{n_h m}{\tau} v &\propto \frac{m}{\tau} n_0 (\mu_+ + \mu_-) \nabla \phi \propto \\ &\frac{\mu_+ + \mu_-}{\mu_h} en_h \nabla \phi \ll en_h \nabla \phi. \end{aligned} \quad (37)$$

Then, in the doped region, Eq. (36) should describe hydrostatic equilibrium for the holes, with balance between electric and pressure forces proportional to $-\nabla \phi$ and $-\nabla n_h$, respectively. However, in the geometry of the doping process, the electric and pressure forces point in the same direction (e.g. to the right in Fig. 1) and therefore *cannot* balance each other. Without the barrier term, Eq. (36) suggests that holes are freely accelerated into the semiconductor, which contradicts the very essence of the doping process. In order to obtain a doping front, one has to balance the electric and pressure forces in Eq. (36) by a counter-term, which takes into account the thermodynamic barrier of the doping process

$$n_h m \frac{d\mathbf{v}}{dt} = -en_h \nabla (\phi - \phi_N) - k_B T \nabla n_h - \frac{n_h m}{\tau} \mathbf{v}. \quad (38)$$

It has been suggested in Ref.²⁸ to consider ϕ_N in the form of the Nernst potential, given by

$$\phi_N(n_h, T) = \frac{k_B T}{e} \ln \left(\frac{n_h}{n_{h,\infty} - n_h} \right), \quad (39)$$

where $n_{h,\infty}$ is the maximal possible concentration of holes. In general, $n_{h,\infty}$ may be larger than the value n_{h1} of the experimentally observed hole concentration behind the p-doping front. For this reason, in the present paper we introduce also a numerical parameter f as $n_{h,\infty} \equiv f n_{h1}$ with $f > 1$. We will show that qualitative properties of the doping front do not depend on the parameter f . As mentioned above, the Nernst potential should be viewed as an injection barrier, and is only described as an electrostatic contribution out of convention. Moreover, the important dynamical aspects of the Nernst potential enter Eq. (36) in the form of a gradient. Since the inclusion of the Nernst potential is formally valid only in the highly doped region, it can therefore be set to an arbitrary constant value in the undoped region, i.e.

$$\phi_N(n_h, T) = 0. \quad (40)$$

A continuous description of the doping front structure also requires a continuous change of the Nernst potential from Eq. (39) to Eq. (40). Since, unfortunately,

there is no theoretical thermodynamic model describing such a transition at present, we introduce a dimensionless phenomenological function ψ with the injection barrier potential given by

$$\phi_N(n_h, T) = \psi \frac{k_B T}{e} \ln \left(\frac{n_h}{n_{h,\infty} - n_h} \right), \quad (41)$$

where $\psi = 1$ in the doped region and $\psi = 0$ in the undoped region. A more detailed form of the function ψ will be discussed below. Taking into account the Nernst potential, Eq. (30) is modified in the doped region according to

$$-n_h U_p + n_h \mu_h E = D_h \left(1 - \psi \frac{f n_{h1}}{f n_{h1} - n_h} \right) \frac{dn_h}{dx}. \quad (42)$$

The set of Eqs. (31), (32), (35), (42) determine the internal structure of the p-doping front.

Another important feature of the system is a strongly nonlinear dependence of the hole mobility on concentration $\mu_h(n_h)$ found experimentally³⁰. Because of this dependence, hole mobility is much larger than the ion mobility in the doped region $\mu_h \gg \mu_{\pm}$, but it becomes much lower $\mu_h \ll \mu_{\pm}$ in the undoped region where $n_h/n_{h1} \ll 1$. The nonlinear dependence is consistent with basic understanding of doping as the process of increasing mobility of charge carriers. Reference²⁸ makes use of the following empirical fit for the hole mobility

$$\mu_h = 3.85 \times 10^{-8} \left[1 + \tanh \left(26.6 \frac{n_h}{n_0} - 4.3 \right) \right], \text{ m}^2/\text{V s}. \quad (43)$$

A similar property holds also for electrons.

B. Dimensionless equations

In order to simplify the analysis, we introduce dimensionless variables for the coordinate, concentrations and electric field: $\xi = x/L_p$, $\alpha_{\pm} = n_{\pm}/n_0$, $\alpha_h = n_h/n_0$, $\varepsilon = E/E_0$. Furthermore, we introduce two parameters specifying ratio of ion mobilities and the front velocity according to

$$\delta = \mu_-/\mu_+, \quad C = \mu_- E_0/U_{p0}. \quad (44)$$

In particular, we have $\delta = 2.2$ for the active material used in the experiments of Refs.^{16,21,28}. In the dimensionless form, the governing equations (42), (31), (32), (35) become

$$\gamma_{eff} \frac{d\alpha_h}{d\xi} = \alpha_h (C M_{1h} \varepsilon - 1), \quad (45)$$

$$\frac{d\alpha_-}{d\xi} = 1 + C - \alpha_- (1 + C\varepsilon), \quad (46)$$

$$\frac{d\alpha_+}{d\xi} = \delta - C - \alpha_+ (\delta - C\varepsilon), \quad (47)$$

$$\alpha_+ - \alpha_- + \alpha_h = 0, \quad (48)$$

where the dimensionless hole mobility and the effective dimensionless hole diffusion are

$$M_h = 175[1 + \tanh(26.6\alpha_h - 4.3)], \quad (49)$$

$$\gamma_{eff} = M_h \left(1 - \frac{\psi \alpha_{h\infty}}{\alpha_{h\infty} - \alpha_h} \right). \quad (50)$$

The numerical solution also requires boundary conditions in the doped region, as specified in Sec. III under a simplifying (though realistic) assumption of infinitely large hole mobility in the doped region, $\mu_{h1} \gg \mu_{\pm}$. Still, it is also useful to determine the boundary conditions without employing such an assumption. The hole concentration in the doped region is known from experiments. Thus, we have to find the ion concentrations in the doped region and the exact value of the C -parameter in Eq. (44), taking into account a finite (though small) electric field ε_1 . Since all derivatives in Eqs. (45)-(47) are zero in the doped region, then we obtain the following boundary conditions

$$\varepsilon_1 = \frac{1}{C M_{1h}}, \quad \alpha_{1-} = \frac{1 + C}{1 + C\varepsilon_1}, \quad \alpha_{1+} = \frac{\delta - C}{\delta - C\varepsilon_1}. \quad (51)$$

Substituting (51) into (48) we find the parameter C

$$C = \frac{\alpha_{1h}}{(\delta + 1)} \left(\delta - \frac{1}{M_{1h}} \right) \left(\frac{1}{M_{1h}} + 1 \right) + \frac{1}{M_{1h}}, \quad (52)$$

where $\alpha_{1h} = n_{1h}/n_0 = 0.277$ determined experimentally. In the limit of infinitely high mobility of holes in the doped region, $M_{1h} \gg 1$, Eq. (52) goes over to Eq. (16), which may be written in the dimensionless form as $C = \alpha_{1h} \delta / (\delta + 1)$. For the experimental values of the hole mobility, the difference between Eqs. (16) and (52) is about 2%. Boundary conditions in the undoped region are, by definition, $\varepsilon_0 = 1$, $\alpha_{0-} = \alpha_{0+} = 1$, $\alpha_{0h} = 0$.

C. Asymptotic behavior in the doped region

We next consider the asymptotic behavior in the specific zones of the front: in the doped region, the undoped region and the transition point between doped and undoped matter. We start with the doped region. Within the limit of high hole mobility, $\mu_{h1} \gg \mu_{\pm}$ i.e. $M_{h1} \gg 1$, we have $\varepsilon_1 = 0$, $\alpha_h = \alpha_{1h}$, $\alpha_{1-} = 1 + \alpha_{1h} \delta / (\delta + 1)$, $\alpha_{1+} = 1 - \alpha_{1h} / (\delta + 1)$ in the doped region at $\xi = -\infty$. We are interested in the asymptotic approach to the doped state, and we investigate small deviations from the limiting values $\varepsilon_1 = \tilde{\varepsilon}$, $\alpha_h = \alpha_{1h} + \tilde{\alpha}_h$, $\alpha_- = \alpha_{1-} + \tilde{\alpha}_-$, $\alpha_+ = \alpha_{1+} + \tilde{\alpha}_+$. We also take into account the Nernst term ($\psi = 1$) in the doped region, which leads to

$$\gamma_{eff} = -M_h \frac{\alpha_h}{f \alpha_{1h} - \alpha_h} \quad (53)$$

in the definition Eq. (50). We immediately see that, in the case of $f = 1$, γ_{eff} diverges in the doped region as $\xi \rightarrow -\infty$. Thus, we have to consider two separate cases of $f > 1$ and $f = 1$ yielding an exponential and a power-law approach to the limiting values, respectively.

We begin with the first case, $f > 1$, for which γ_{eff} is a constant coefficient in Eqs. (45)-(48), $\gamma_{eff} = -M_h/(f-1)$. Linearizing Eqs. (45)-(48) with respect to small deviations in the doped region, we obtain

$$-\frac{1}{f-1} \frac{d\tilde{\alpha}_h}{d\xi} = \frac{\alpha_{1h}^2 \delta}{\delta+1} \tilde{\varepsilon}, \quad (54)$$

$$\frac{d\tilde{\alpha}_-}{d\xi} = -\tilde{\alpha}_- - \left(1 + \frac{\alpha_{1h}\delta}{\delta+1}\right) \frac{\alpha_{1h}\delta}{\delta+1} \tilde{\varepsilon}, \quad (55)$$

$$\frac{d\tilde{\alpha}_+}{d\xi} = -\tilde{\alpha}_+\delta + \left(1 - \frac{\alpha_{1h}}{\delta+1}\right) \frac{\alpha_{1h}\delta}{\delta+1} \tilde{\varepsilon}, \quad (56)$$

$$\tilde{\alpha}_+ - \tilde{\alpha}_- + \tilde{\alpha}_h = 0. \quad (57)$$

The system of Eqs. (54)-(57) has an exponential solution in the form $\tilde{\varepsilon} \propto \tilde{\alpha}_h \propto \tilde{\alpha}_- \propto \tilde{\alpha}_+ \propto \exp(\chi\xi)$ with positive eigenvalues χ corresponding to the exponent decay at $\xi \rightarrow -\infty$. In general, the eigenvalue may be calculated numerically. Still, we can find an analytical solution to the system in the most important limit of $f-1 \ll 1$, which describes the most interesting features of the front in the doped region. Substituting the deviations of electric field $\tilde{\varepsilon}$ from Eq. (54) into Eqs. (55) and (56), we obtain

$$\frac{d\tilde{\alpha}_-}{d\xi} = -\tilde{\alpha}_- + \left(1 + \frac{\alpha_{1h}\delta}{\delta+1}\right) \frac{1}{(f-1)\alpha_{1h}} \frac{d\tilde{\alpha}_h}{d\xi}, \quad (58)$$

$$\frac{1}{\delta} \frac{d\tilde{\alpha}_+}{d\xi} = -\tilde{\alpha}_+ - \frac{1}{\delta} \left(1 - \frac{\alpha_{1h}}{\delta+1}\right) \frac{1}{(f-1)\alpha_{1h}} \frac{d\tilde{\alpha}_h}{d\xi}. \quad (59)$$

Thus, in the case of $f-1 \ll 1$, taking the difference of Eqs. (55) and (56) and accounting for Eq. (57) we find that

$$\tilde{\alpha}_h = \frac{\delta+1 + \alpha_{1h}(\delta-1)}{\delta(f-1)\alpha_{1h}} \frac{d\tilde{\alpha}_h}{d\xi}, \quad (60)$$

with the eigenvalue

$$\chi = \frac{\delta\alpha_{1h}(f-1)}{\delta+1 + \alpha_{1h}(\delta-1)}. \quad (61)$$

For the experimental data $\alpha_{1h} = 0.277$ and $\delta = 2.2$ we find that relaxation of the parameters to the saturation values in the p-doped region occurs on a length scale $\approx 7.1L_p/(f-1)$. Therefore, in the limit of $f-1 \ll 1$, the relaxation happens on length scales much greater than the characteristic length L_p , Eq. (33), related to ion diffusion. We stress also that without employing the

injection barrier in the doped region [i.e. taking $\psi = 0$ in Eq. (40)], we do not find any deviation mode vanishing asymptotically to $\xi \rightarrow -\infty$ in agreement with the previous numerical results²⁸. The physical meaning of this effect was explained above in Sec. IV A.

The relaxation process goes even slower in the specific case of $f = 1$, when Eq. (54) becomes intrinsically nonlinear

$$\frac{1}{\tilde{\alpha}_h} \frac{d\tilde{\alpha}_h}{d\xi} = \frac{\alpha_{1h}\delta}{\delta+1} \tilde{\varepsilon}. \quad (62)$$

Then, instead of Eq. (60), we obtain

$$\frac{d\tilde{\alpha}_h}{d\xi} = -\frac{\tilde{\alpha}_h^2 \delta}{\delta+1 + \alpha_{1h}(\delta-1)}, \quad (63)$$

with the asymptotic solution

$$\tilde{\alpha}_h = \frac{\delta+1 + \alpha_{1h}(\delta-1)}{\xi\delta} \quad (64)$$

for $\xi \rightarrow -\infty$. According to Eq. (64), in the case of $f = 1$ the relaxation of the hole concentration goes inversely proportional to the distance from the doping front. Such behavior is much slower than the exponential law predicted by Eq. (60) for $f > 1$.

Thus, we obtain a smooth relaxation of the p-front parameters to the final values in the doped region on the length scales much larger than L_p , Eq. (33), determined by ion diffusion.

D. Asymptotic behavior in the undoped region

In this subsection we study the asymptotic front structure in the undoped region ($\xi \rightarrow \infty$) with $\varepsilon_0 = 1$, $\alpha_{0-} = \alpha_{0+} = 1$, $\alpha_{0h} = 0$, $\psi = 0$ in the limit $\gamma_{eff} = M_{h0} \ll 1$, the latter due to the strongly nonlinear dependence of hole mobility on concentration, Eq. (43). Using again a tilde to denote the deviation variables, Eqs. (45)-(48) may be linearized with respect to small deviations to give

$$M_{h0} \frac{d\tilde{\alpha}_h}{d\xi} = -\tilde{\alpha}_h, \quad (65)$$

$$\frac{d\tilde{\alpha}_-}{d\xi} = -\tilde{\alpha}_- \left(1 + \frac{\alpha_{1h}\delta}{\delta+1}\right) - \frac{\alpha_{1h}\delta}{\delta+1} \tilde{\varepsilon}, \quad (66)$$

$$\frac{d\tilde{\alpha}_+}{d\xi} = -\tilde{\alpha}_+ \left(\delta - \frac{\alpha_{1h}\delta}{\delta+1}\right) + \frac{\alpha_{1h}\delta}{\delta+1} \tilde{\varepsilon}, \quad (67)$$

$$\tilde{\alpha}_+ - \tilde{\alpha}_- + \tilde{\alpha}_h = 0. \quad (68)$$

The system (65)-(68) has two independent modes in the form of $\tilde{\varepsilon} \propto \tilde{\alpha}_h \propto \tilde{\alpha}_- \propto \tilde{\alpha}_+ \propto \exp(\chi\xi)$ decaying exponentially at $\xi \rightarrow \infty$ with $\chi < 0$. One mode is related to the perturbations of the holes, $\tilde{\alpha}_h \neq 0$, with the eigenvalue

$$\chi = -1/M_{h0}, \quad (69)$$

which is obtained in a straightforward way from Eq. (65). In the limit of ultimately low hole mobility in the undoped region, $M_{h0} \ll 1$, this mode is characterized by extremely sharp gradients, thus leading to a steep head of the front with an associated length scale $\approx M_{h0}L_p$, which is much smaller than the length scale L_p due to ion diffusion. This mode is also expected to lead to a sharp peak in the electric field, which is proportional to the gradient of hole concentration according to

$$\frac{d\tilde{\alpha}_h}{d\xi} = -2 \frac{\alpha_{1h}\delta}{\delta+1} \tilde{\varepsilon}. \quad (70)$$

The second mode in the undoped region happens with zero deviations of the hole concentration, $\tilde{\alpha}_h = 0$, and equal non-zero deviations for the ion concentrations, $\tilde{\alpha}_- = \tilde{\alpha}_+ \neq 0$. Then Eqs. (66), (67) yield

$$\frac{d\tilde{\alpha}_{\pm}}{d\xi} = -\frac{1+\delta}{2} \tilde{\alpha}_{\pm} \quad (71)$$

with the eigenvalue

$$\chi = -\frac{1+\delta}{2}. \quad (72)$$

The second mode is controlled by ion diffusion with the typical length scale comparable to L_p . Because of the second mode one should expect a non-monotonic behavior of the ion concentrations in the doped region. After sharp changes related to the first mode with complete vanishing of the hole concentration, a relatively slow relaxation of ions to $\alpha_{0-} = \alpha_{0+} = 1$ is thus expected.

E. Behavior in the transition point

The solution to the system (45)-(48) demonstrates that the doping front possesses one more specific point, which indicates transition from the doped to undoped zones. This point gives the answer to the question where the injection barrier (the Nernst term) should be switched off via the phenomenological parameter ψ going over from 1 to 0. *A priori*, it is natural to expect the critical point to be in the region where the hole mobility becomes comparable to the ion mobility. However, it turns out that the system specifies an *exact* position of the critical transition point (which we label by c) characterized by zero derivatives of Eqs. (45)-(48), i.e.

$$0 = \frac{\alpha_{1h}\delta}{\delta+1} M_h(\alpha_{hc}) \varepsilon_c - 1, \quad (73)$$

$$0 = 1 + \frac{\alpha_{1h}\delta}{\delta+1} - \alpha_{c-} \left(1 + \frac{\alpha_{1h}\delta}{\delta+1} \varepsilon_c \right), \quad (74)$$

$$0 = \delta - \frac{\alpha_{1h}\delta}{\delta+1} - \alpha_{c+} \left(\delta - \frac{\alpha_{1h}\delta}{\delta+1} \varepsilon_c \right), \quad (75)$$

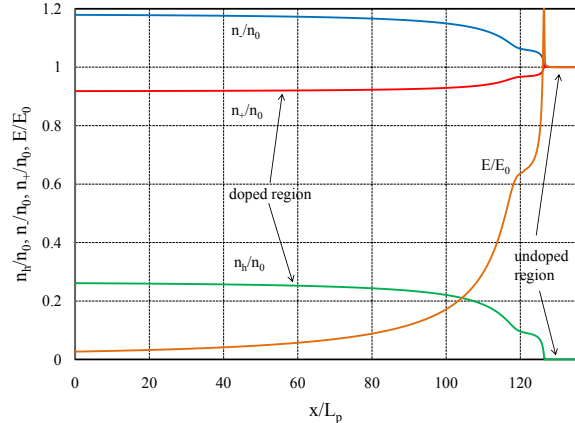


FIG. 3. Concentrations of holes and ions, and the electric field inside the p-doping front; $f = 1.1$.

$$\alpha_{c+} - \alpha_{c-} + \alpha_{hc} = 0. \quad (76)$$

Due to the essentially nonlinear dependence of hole mobility on concentration, see Eq. (43), the set of equations (73)-(76) is also strongly nonlinear and it can only be solved numerically. Thus, solving Eqs. (73)-(76) for the experimentally obtained parameters $\alpha_{1h} = 0.277$ and $\delta = 2.2$, we find the critical point at $\alpha_{hc} \approx 0.092$, $M_h(\alpha_{hc}) = \mu_h/\mu_- \approx 8.5$ with the scaled electric field at that point calculated as $\varepsilon_c \approx 0.65$ from Eq. (73).

The critical point has an interesting physical meaning. Going back to the dimensional equations for the front structure, Eqs. (30)-(32), and setting all derivatives equal to zero, we find the critical point corresponding to

$$-U_p + \mu_h E = 0. \quad (77)$$

Thus, at the critical point we obtain holes moving locally with the same velocity $\mu_h E$ as the p-doping front, which may be also interpreted as a “resonance” between the light charges and the front. To the left of this point (in the doped region) hole mobility may provide faster velocity of the particles in comparison with the front. To the right of the critical point, hole mobility is too low for holes to keep up with the front velocity. Therefore the critical point plays the natural role of a border between the doped and undoped regions.

F. Numerical solution for the front structure

In this section, we solve Eqs. (45)-(50) numerically with the boundary conditions ahead of the doping front and behind the front as obtained in Sec. IV B. Figure 3 shows the internal structure of a stationary p-doping front in terms of the normalized concentrations of holes,

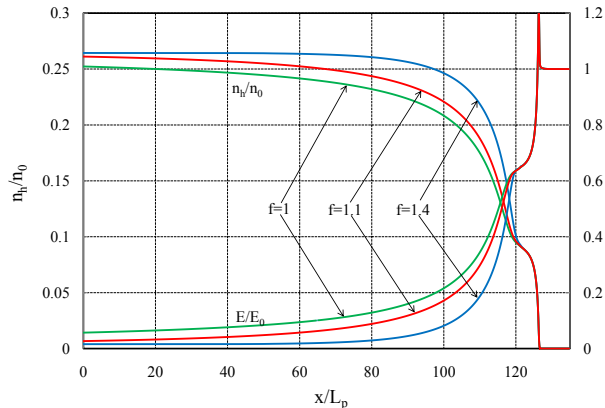
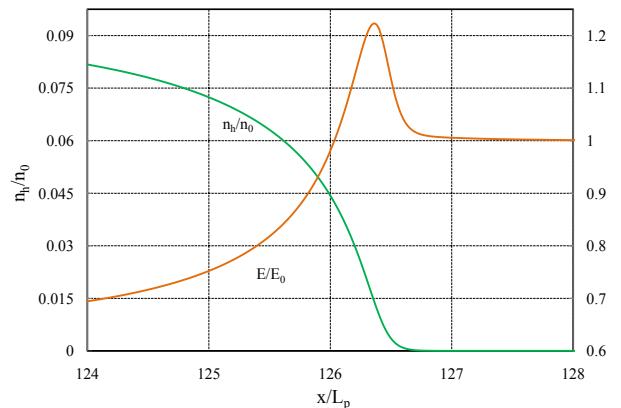


FIG. 4. Concentration of holes and the electric field inside the p-doping front for different values of the f -factor.

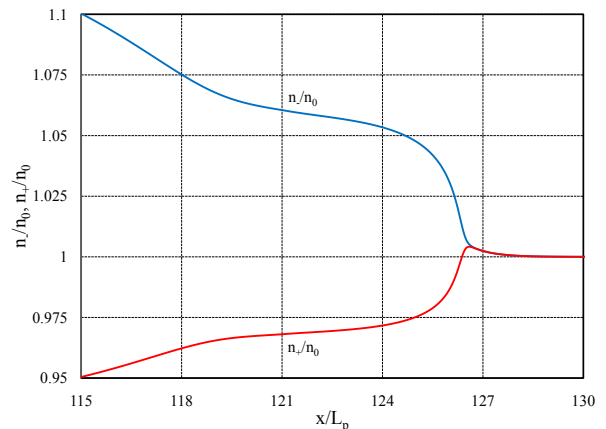
positive and negative ions and the electric field as a function of distance. The front propagates to the right converting the undoped semiconductor material with low conductivity to the doped one with high conductivity. In agreement with the analysis of Subsections IV C-E, the whole doping front has a complicated nonlinear structure with several specific zones characterized by different length scales. The length scale variations within the front are related, first of all, to dramatic changes of the hole mobility by three orders of magnitude from the undoped to doped regions. We point out a sharp head of the front in the undoped region, an extremely smooth relaxation tail in the doped region and an additional plateau connecting these two regions. The length scale variations inside the doping front resemble a similar effect encountered in laser deflagration, where the length scale may also change by several orders of magnitude within the deflagration front due to electron heat conduction increasing strongly with temperature³¹.

As explained in Sec. IV C, the smooth relaxation tail in the doped region is due to high mobility of holes in that region and the Nernst term modeling the injection barrier. The numerical solution shown in Fig. 3 uses the parameter value $f = 1.1$, which provides the characteristic length scale $\approx 71L_p$ of the relaxation. Indeed, in Fig. 3 we see that the relaxation length scale in the doped region exceeds the length scale of ion diffusion L_p by approximately two orders of magnitude. Figure 4 shows modifications of the front structure caused by changing of the parameter f . In agreement with the theoretical predictions, relaxation to the final doped state becomes smoother as f approaches unity. At the same time, the parameter f does not influence the head of the front.

The details of the p-front structure in the undoped region (head of the front) are shown in Fig. 5. Figure 5(a) presents the concentration of holes and the electric



(a)



(b)

FIG. 5. Structure of the p-front in the undoped region, (a) hole concentration and the electric field, (b) ion concentrations.

field. In agreement with the asymptotic theory of Sec. IV D, we can see sharp gradients of the hole concentration with characteristic length scales noticeably smaller than the length scale L_p of ion diffusion. The theory predicts that the electric field in the leading part of the front is proportional to the spatial derivative of the hole concentration, see Eq. (70), which leads to a sharp peak in the electric field clearly visible in Fig. 5(a). Figure 5(b) shows the variations of the ion concentration at the head of the doping front. Unlike the hole concentration, the concentrations of ions demonstrate a more complicated behavior. First, the two ion concentrations approach each other on a short length scale related to the mode with the eigenvalue given by Eq. (69). However,

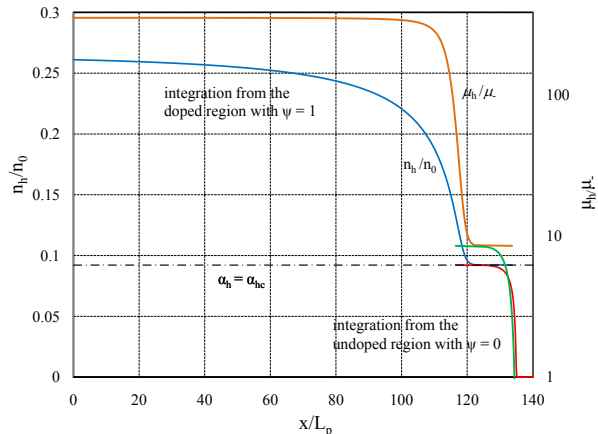


FIG. 6. Hole concentration and mobility inside the p-doping front obtained by integration from the doped region (left) with the Nernst term and from the undoped region (right) without the Nernst term.

instead of a monotonic relaxation to the limiting values, the concentration n_+ overshoots n_0 , so that n_- and n_+ meet at some value exceeding n_0 (in agreement with the constraint of quasi-neutrality). After that, both the ion concentrations n_- and n_+ approach the limiting value n_0 together from above. Such a specific way of relaxation for the ion concentrations is in agreement with the second mode, as given by Eq. (72), predicted analytically in Sec. IV D. The ion relaxation is of course determined by ion diffusion and occurs on length scales comparable to L_p .

The specific behavior of the doping front parameters close to the critical point is another interesting feature of the system. The critical point was not discussed in Ref.²⁸, since in that work a matching of the concentration gradients was done by a linear extrapolation from the doped and undoped regions. However, we stress that the critical point is *not* a mathematical artifact of the phenomenological transition function ψ . As demonstrated in Sec. IV E, the local velocity of holes produced by their mobility is in resonance with the p-front velocity in the critical point, and this resonance explains the physical origin of the critical point and the zone around it. In order to understand the effect of this critical zone better, we may integrate Eqs. (45)-(50) in two opposite directions: from the doped region with $\psi = 1$ (from left to right in Fig. 3) and from the undoped region with $\psi = 0$ (from right to left in Fig. 3). Figure 6 presents the concentration of holes and the hole mobility obtained from such an integration procedure. As illustrated in Fig. 6, integrating from the doped region we could not reach the undoped one, and vice versa. Instead, using both ways of integration we reach asymptotically the critical point as a saturation limit: from above for $\psi = 1$ and from

below for $\psi = 0$. From the mathematical point of view, passing the critical resonance point means changing sign of the right-hand side of Eq. (45), $(CM_h\varepsilon - 1)$. The continuous transition from the doped (left) to undoped (right) regions requires a non-positive derivative of the hole concentration, $d\alpha_h/d\xi$, and, therefore, the effective hole diffusion γ_{eff} has to change sign in the critical point. We remind that the effective diffusion is a combination of the real diffusion and the Nernst contribution describing the injection barrier. The role of the Nernst term is controlled by the phenomenological function ψ , which therefore has to change from 1 (the Nernst term is then switched on) to 0 (the Nernst term is switched off) in the vicinity of the critical point. For example, matching the concentration profiles obtained by integration from the right and from the left at the critical point we find the front structure for $\psi(n_h)$ in the form of a step-function. Still, a smooth transition function is required for treating the doping fronts numerically within the evolution problems. Due to the lack of a good thermodynamic model for the transition from the undoped to doped state, we use the following phenomenological form of the transition function:

$$\psi = 0.5 + 0.5 \tanh [A_1 (CM_h\varepsilon - 1) |CM_h\varepsilon - 1|^n + 0.5 \ln (\alpha_{h\infty}/\alpha_h - 1)]. \quad (78)$$

The hyperbolic tangent of Eq. (78) provides a smooth transition from 1 to 0 for ψ as we go from the doped to undoped region. The function Eq. (78) depends on the combination $(C\mu_h\varepsilon - 1)$, which is the right side of Eq. (45). When this combination is zero, the residual term makes $\gamma_{eff} = 0$ and allows for a smooth change in all the concentrations. The other parameters of the transition function are chosen to reduce the plateau near the critical point. In our calculations presented in Fig. 3 we used $A_1 = 8$ and $n = 0.1$. Hypothetically, a transition function ψ may exist, which eliminates the plateau completely. However, we believe that it is important to obtain the transition function from first principles of thermodynamics and quantum mechanics, rather than to make a more elaborate phenomenological construction. This is indeed an important and difficult problem left for the future, while at present we simply use a phenomenological function for ψ to obtain a smooth transition through the critical point from the undoped to doped region.

All the main characteristic features of the doping front for holes are relevant for electron doping as well. In Fig. 7 we depict the stationary doping front for electrons (the n-front). The characteristic length scale related to the n-doping front is defined in the same way as for the p-front according to

$$L_n = \frac{D_-}{U_{n0}} = \frac{D_- n_{1e}}{(\mu_+ + \mu_-) n_0 E_0}. \quad (79)$$

In order to obtain a numerical result for the front structure we used the electron mobility function

$$M_h = 145[1 + \tanh(21.6\alpha_h - 4.3)] \quad (80)$$

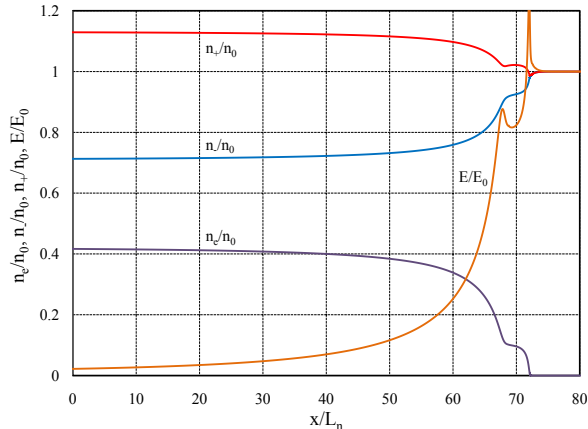


FIG. 7. Concentrations of electrons and ions, and the electric field inside the n-doping front.

constructed from the experimental data^{13,30}, and the phenomenological transition function similar to the one given in Eq. (78), i.e.

$$\psi_e = 0.5 + 0.5 \tanh \left[14.4 (CM_e \varepsilon - 1) |CM_e \varepsilon - 1|^{0.1} + 0.5 \ln (\alpha_{e\infty}/\alpha_e - 1) \right]. \quad (81)$$

The electron mobility in OSCs is somewhat lower than the hole mobility. Similar to the p-front shown in Fig. 3, the n-doping fronts have also very elongated tails in the doped region, a sharp head with a peak of the electric field in the undoped region and a critical point of transition from the undoped to doped state at $\mu_e/\mu_- \approx 3.5$. We point out that the critical point for electrons corresponds to considerably lower mobility (the critical point for holes is achieved at $\mu_h/\mu_- \approx 8.5$). Because of the lower electron mobility, the critical point demonstrates a more complicated structure for the n-front in comparison with the p-front. In the case of the p-front, saturation of all the concentrations and the electric field to the plateau of the critical point occurs monotonically, see Fig. 6. On the contrary, in the case of the n-doping front presented in Fig. 7, the concentration of positive ions and the electric field exhibit a non-monotonic behavior when approaching the plateau. This behavior shows clearly existence of two perturbation modes in the doped zone close to the critical point, which resemble qualitatively the modes obtained in Sec. IV D. We have found a qualitatively similar structure of the transition zone for several types of function ψ .

An interesting consequence of the above discussion of the critical point is the possibility of a weak doping process, when the final concentration of the light charge carrier is still smaller than the corresponding critical value. Such a doping front can be described without the Nernst potential and the transitional function. At the same

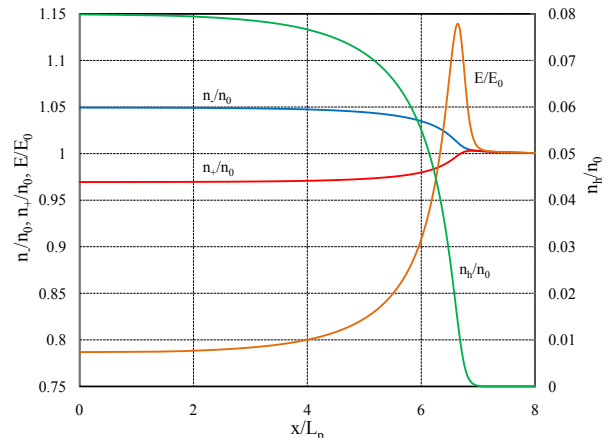


FIG. 8. Concentrations of holes and ions, and the electric field inside the p-front of weak doping for $n_{1h}/n_0 = 0.08$.

time, the front structure in the undoped region remains the same as described in Sec. IV D. The p-front of such a weak doping transformation is shown in Fig. 8; it is similar to the right part (head) of the front in Figs. 3 and 6. The final hole concentration in Fig. 8 is smaller than the critical one, namely, $\alpha_{1h} = 0.08$, and the corresponding final mobility of the holes is $\mu_{1h}/\mu_0 = 4.5$. As the hole mobility is about 80 times smaller than in fully doped case, then, according Eq. (77), the final electric field remains relatively large behind the front, $\varepsilon_1 \approx 0.8$, though smaller than the initial one, $\varepsilon_0 = 1$. The total length of the front is much shorter than the front width in Fig. 3, as the long relaxation tail in the strongly doped region is missing here. In general, the front of weak doping transformation may be interpreted as a part of the complete doping front from the head to the critical point.

Finally, we present the structure of the p- and n-doping fronts as they accelerate towards each other in Fig. 9. Since the characteristic time scales related to the fronts (that is $\tau_p \propto L_p/U_p = D_-/U_p^2$ and $\tau_n \propto L_n/U_n = D_-/U_n^2$) are much smaller than the time of the front acceleration, then the structure may be obtained within the quasi-classical Wentzel-Kramers-Brillouin approximation. Within this approximation, structure of the fronts remains self-similar, but the length scales L_p and L_n decrease due to the increase of the electric field and the front velocities U_p and U_n as discussed in Sec. III.

V. CONCLUSIONS

In this paper we have investigated the dynamics and internal structure of the planar p- and n-type doping fronts in organic semiconductors with applications to LECs. The study is based on the drift-diffusion model

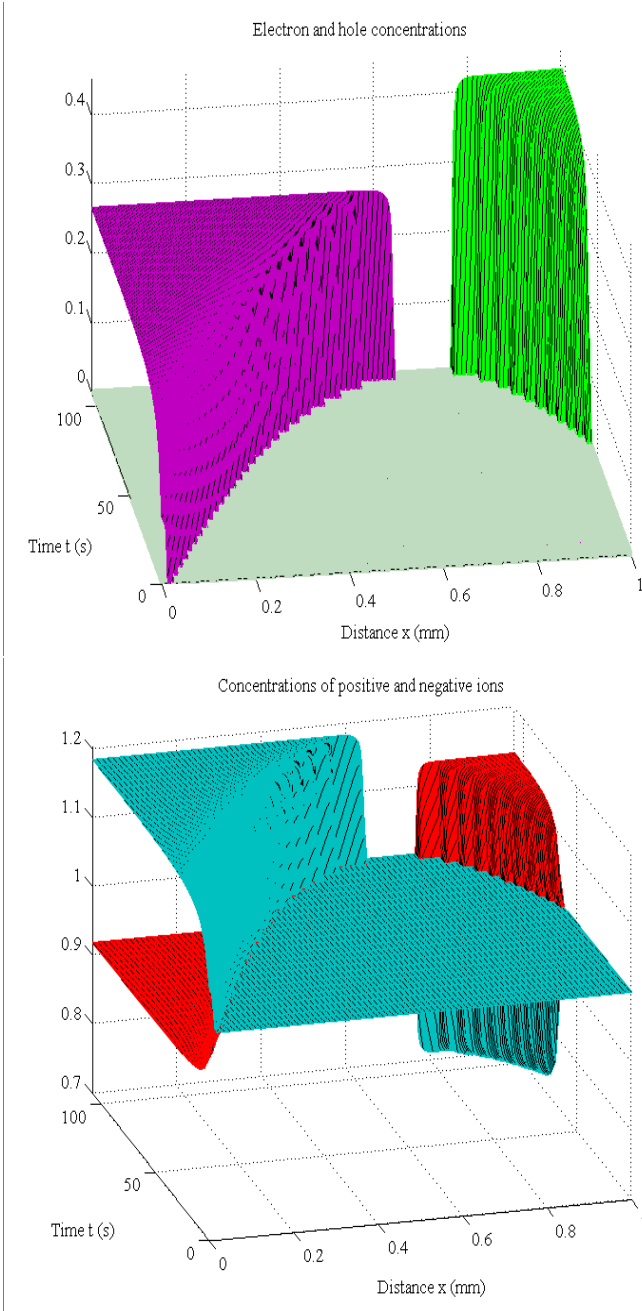


FIG. 9. The p- and n- fronts accelerating towards each other. (a) hole and electron concentrations are depicted by magenta and green, (b) negative and positive ions are shown by blue and red.

taking into account the injection barrier and a strongly nonlinear dependence of the hole and electron mobility/diffusion on concentration, following the work Ref. 28. A similar model has been employed before to describe transformation fronts in one-electrode devices like electrochemical sensors and actuators in Ref. 27. Still, there is an important difference between these two types

of processes/devices. In the doping front (studied in the present paper) holes and electrons populate the active material while ions give way to the light charges. As a result, conductivity of the material *increases* drastically, by 2-3 orders of magnitude. On the contrary, the transformation fronts in ambipolar devices imply that cations replace holes with strong *decrease* of conductivity. The different characters of the processes lead naturally to different properties of the transformation fronts.

Here we have studied parameters of the doping fronts on different scales, both within the discontinuous front approach and also by taking into account the internal front structure. Within the limit of a discontinuous front we have derived the analytical formulas for the front velocities, the ion concentrations in the doped region, and described dynamics of the p- and n-doping fronts accelerating towards each other in LECs. The analytical results for the planar front dynamics are in a good quantitative agreement with the experimental data for the slowest part of the experimentally observed front brush. We remind that experiments demonstrate also a complicated multidimensional front dynamics related to instabilities. Theoretical investigation of the front instabilities is beyond the scope of this paper and is presented elsewhere²⁹.

One of the main purposes of the present paper was to investigate the internal structure of the doping fronts. In agreement with the previous ideas²⁸, we show that continuous transition from the doped to undoped state in the form of a moving front requires a thermodynamic injection barrier and a nonlinear dependence of the hole/electron mobility on concentration, which is quite in line with the basic principles of the doping process. We have studied the asymptotic behavior of the front parameters: 1) relaxation to the doped state at the back of the front, 2) deviation from the undoped state at the head of the front and 3) the critical point of the transition from the doped to undoped parts of the front, where the velocity of the light charges are in resonance with the front speed. We have also obtained a numerical solution for the front structure. Both the analytical theory and the numerical solution demonstrated the multi-scale features of the doping fronts, which include an extremely smooth relaxation tail in the doped region, a sharp head of the front with large gradients in the undoped zone, and a plateau at the critical point. The described front structure agrees qualitatively with observations of the previous experiments²⁸.

ACKNOWLEDGMENTS

The authors are grateful to Ludvig Edman and Piotr Matyba for numerous discussions and the experimental data. This work was supported by the Swedish Research Council (VR) and by the Kempe Foundation.

- * E-mail address: mattias.marklund@physics.umu.se
- ¹ G. Malliaras, R. Friend, *Phys. Today* **58**(5), 53 (2005).
 - ² H. Sirringhaus, N. Tessler, R. N. Friend, *Science* **280**, 1741 (1998).
 - ³ A. J. Heeger, *Rev. Mod. Phys.* **73**, 681 (2001).
 - ⁴ S. R. Forrest, *Nature* **428**, 911 (2004).
 - ⁵ M. J. Leger, *Adv. Mater.* **20**, 837841 (2008)
 - ⁶ C. K. Chiang, C. R. Fincher, Y. W. Park, A. J. Heeger, H. Shirakawa, E. J. Louis, S. C. Gau, and A. G. Macdiarmid, *Physical Review Letters* **39**, 1098 (1977).
 - ⁷ Y. Li, Y. Cao, J. Gao, D. Wang, G. Yu, A. J. Heeger, *Electrochemical Synthetic Metals* **99**, 243 (1999).
 - ⁸ Q. B. Pei, Y. Yang, G. Yu, C. Zhang, and A. J. Heeger, *Journal of the American Chemical Society* **118**, 16, 3922 (1996).
 - ⁹ P. Matyba, M. R. Andersson, L. Edman, *Organic Electronics*, **9**, 699 (2008).
 - ¹⁰ Q. B. Pei, G. Yu, C. Zhang, Y. Yang, A. J. Heeger, *Science* **269**, 1086 (1995).
 - ¹¹ V. Coropceanu, J. Cornil, D. A. da Silva, Y. Olivier, R. Silbey, and J. L. Bredas *Chem. Rev.* **107**, 926 (2007).
 - ¹² J. L. Bredas, J. P. Calbert, D. A. da Silva, J. Cornil, *PNAS* **99** (9), 5804 (2002).
 - ¹³ V. I. Arkhipov, E. V. Emalianova, P. Heremans, H. Bassler *Phys. Rev. B* **71**, 235202 (2005).
 - ¹⁴ Q. B. Pei, Y. Yang, G. Yu, Y. Cao, and A. J. Heeger, *Synthetic Metals* **85**, 1229 (1997).
 - ¹⁵ Q. J. Sun, Y. F. Li, and Q. B. Pei, *Journal of Display Technology* **3**, 211 (2007).
 - ¹⁶ P. Matyba, K. Maturova, M. Kemerink, N. D. Robinson, L. Edman, *Nature Mater.* **8**, 672 (2009).
 - ¹⁷ S. van Reenen, P. Matyba, A. Dzwilewski, R. A. J. Janssen, L. Edman, and M. Kemerink, *J. Am. Chem. Soc.* **132**, 13776 (2010).
 - ¹⁸ J. Gao and J. Dane, *Appl. Phys. Lett.* **84**, 2778 (2004).
 - ¹⁹ Y. F. Hu, C. Tracy, and J. Gao, *Appl. Phys. Lett.* **88** (2006).
 - ²⁰ T. Johansson, N. K. Persson, O. Inganäs, *J. Electrochem. Soc.* **151**, E119 (2004).
 - ²¹ N. Robinson, J. H. Shin, M. Berggren M., L. Edman, *Phys. Rev. B* **74**, 155210 (2006).
 - ²² D. L. Smith, *J. Appl. Phys.* **81**, 2869 (1997).
 - ²³ J. A. Manzanares, H. Reiss, A. J. Heeger, *J. Phys. Chem. B* **102**, 4327 (1998).
 - ²⁴ J.C. Lacroix, K. Fraoua, P.C. Lacaze, *J. Electroan. Chem.* **444**, 83 (1998).
 - ²⁵ F. Miomandre, M.N. Bussac, E. Vieil, L. Zuppiroli, *Chem. Phys.* **255**, 291 (2000).
 - ²⁶ X. Wang, B. Shapiro, E. Smela, *Adv. Mater.* **16**, 1605 (2004).
 - ²⁷ X. Wang, B. Shapiro, E. Smela, *J. Phys. Chem. C* **113**, 382 (2009).
 - ²⁸ M. Modestov, V. Bychkov, G. Brodin, D. Valiev, M. Marklund, P. Matyba, L. Edman, *Phys. Rev. B* **81**, 081203(R) (2010).
 - ²⁹ V. Bychkov, P. Matyba, V. Akkerman, M. Modestov, D. Valiev, G. Brodin, C.K. Law, M. Marklund, L. Edman, *submitted*.
 - ³⁰ H. Shimotani, G. Diguët, and Y. Iwasa, *Appl. Phys. Lett.* **86**, 022104 (2005).
 - ³¹ M. Modestov, V. Bychkov, D. Valiev, M. Marklund, *Phys. Rev. E* **80** 046403 (2009).